Adhesion, friction and wear on the nanoscale of MWNT tips and SWNT and MWNT arrays

2008 Nanotechnology 19 125702

(http://iopscience.iop.org/0957-4484/19/12/125702)

Nanotechnology **19** (2008) 125702 (10pp) doi:10.1088/0957-4484/19/12/125702

Adhesion, friction and wear on the nanoscale of MWNT tips and SWNT and MWNT arrays

Bharat Bhushan[1], **Barbara Galasso**[2], **Cristina Bignardi**[2], **Cattien V Nguyen**[3], **Liming Dai**[4] **and Liangti Qu**[4]

[1] Nanotribology Laboratory for Information Storage and MEMS/NEMS, 201 West 19th Avenue, Ohio State University, Columbus, OH 43210-1142, USA
[2] Politecnico di Torino, Dipartimento di Meccanica, Corso Duca degli Abruzzi 24, 10129 Torino, Italy
[3] ELORET NASA Ames Research Center, MS 229-1, Moffet Field, CA 94035, USA
[4] Department of Chemical and Materials Engineering, University of Dayton Research Institute, 300 College Park, Dayton, OH 45469, USA

Received 30 October 2007, in final form 8 January 2008
Published 21 February 2008
Online at stacks.iop.org/Nano/19/125702

Abstract
The nanotribological characterization of carbon nanotubes is fundamental for the exploration of new sliding applications. In this study, a comprehensive investigation of adhesion, friction and wear of a multiwalled nanotube (MWNT) tip, and SWNT (single-walled nanotube) and MWNT arrays has been carried out. A nonlinear response of the MWNT tip is observed when the tip is brought into and out of contact with various surfaces. A nonlinear response occurs due to the buckling of the nanotube and its subsequent sliding on the surface. In addition to the role of surface chemistry, it can also explain the relatively high value of the coefficient of friction obtained on different surfaces, as compared to that of Si and Si_3N_4 tips. The adhesion and friction studies carried out on SWNT and MWNT arrays using Si tips show that SWNT arrays, compared to MWNT arrays, exhibit lower values, possibly due to lower van der Waals forces as a result of lower packing density and higher flexibility. The wear tests conducted with the MWNT tip and a Si tip on a gold film, at two normal loads, show less damage of the surface when the MWNT tip is used because of the MWNT acting as a compliant spring, absorbing part of the load. Wear tests conducted with a Si tip on SWNT and MWNT arrays show that the arrays do not wear. The tip wear and the friction force in the SWNT array are lower, because of lower adhesion and higher flexibility of the SWNTs, which causes less opposition to the motion of the tip.

1. Introduction

Carbon nanotubes (CNTs) were discovered in 1991 by Iijima (1991). They exist in three forms: single-walled nanotubes (SWNTs) constituted of one atomic plane of carbon atoms perfectly rolled into a cylinder; double-walled nanotubes (DWNTs) formed by two layers of graphene (sheets of graphite-like arrangements of C atoms); multiwalled nanotubes (MWNTs), characterized by concentric cylindrical shells of graphene, where the intershell interaction is predominantly van der Waals (Dresselhaus *et al* 2000). Since their discovery, researchers have been studying these nanometer-scale structures and have discovered their extraordinary properties. Due to their unique molecular structure, outstanding electrical properties, good chemical stability and excellent mechanical properties, carbon nanotubes seem promising for a variety of applications. Large-scale production of such nanostructures was started by Ebbesen and Ajayan (1992), and followed by Iijima and Ichihashi (1993) and others, due to the large interest related to this new material. In 1995, de Heer and his co-workers (de Heer *et al* 1995) developed the first method to vertically align the nanotubes. Both the research and industrial attention is focused on the production of individual nanotubes, as well as ceramics, metals and polymer composites with CNT arrays. Carbon nanotubes are of great importance for various applications, which include field

emitters, molecular transistors, electrode devices for flat panel displays, batteries, microfluidics, biosensors, functionalized devices for biomedical and optoelectronic applications, nanotweezers, biomimetics and fillers in nanocomposites (Kim and Lieber 1999, Kong *et al* 2000, Nygård *et al* 2000, Nakayama and Akita 2001, Baughman *et al* 2002, Dai *et al* 2003, Bhushan 2007).

Because of their small radii and their high mechanical robustness, individual carbon nanotubes are well suited for use as atomic force microscopy (AFM) probes (Dai *et al* 1996, Snow *et al* 2002, Bhushan *et al* 2004). In fact, the cylindrical shape and the small diameter of the nanotubes enable imaging in narrow, deep crevices, and improve lateral resolution in comparison to conventional AFM probes (Nguyen *et al* 2004).

Due to their mechanical strength, combined with their low density, carbon nanotubes seem to be the optimal fillers in composites with various materials. Different studies have demonstrated that the use of carbon nanotubes in polymeric matrices can considerably improve the mechanical and tribological properties of the composites (Schadler *et al* 1998, Quian *et al* 2000, Biercuk *et al* 2002, Shi *et al* 2003, Li *et al* 2004, Yang *et al* 2005, Lee *et al* 2007). CNT–metallic composites are interesting because of their high wear resistance (Dong *et al* 2001, Chen *et al* 2003, Wang *et al* 2003, Chen *et al* 2006, Zhou *et al* 2007), and their thermal properties, making them suitable for high thermal management of high-power devices (Pambaguian *et al* 2007). Carbon nanotubes have also been added to ceramic matrices. In particular, it has been shown that they can improve the elastic deformation characteristics and the fracture toughness of SiC and alumina matrices (Siegel *et al* 2001, Peigney *et al* 2002, An *et al* 2003, Pambaguian *et al* 2007).

The vertical orientation of CNTs with respect to the substrate is used to increase the field emission of such nanostructures (Fan *et al* 1999, Chen *et al* 2000, Nakayama and Akita 2001), and it can also affect their thermal properties (Shaikh *et al* 2007). It is then of interest to study aligned nanotube arrays and create nanofiber structures using CNT arrays for various applications, including mimicking gecko feet and the lotus effect (Lau *et al* 2003, Yurdumakan *et al* 2005, Huang *et al* 2005, Zhu *et al* 2005).

Focusing on the CNT tips, scanning probe studies have been conducted in tapping mode. Nguyen *et al* (2001) analyzed the stability and the lateral resolution capability of CNT scanning probes applied to AFM, using an MWNT probe and an SWNT probe. By imaging in tapping mode, they compared the resolution reachable using CNT tips or conventional silicon probes. With this work, Nguyen and co-workers illustrated how the MWNT probe does not degrade after a long period of continuous scanning (more than 15 h) and how the SWNT probe is capable of lateral resolution as small as 2 nm. Larsen *et al* (2002) compared the wear and degradation of conventional commercial etched silicon probes with those of multiwalled carbon nanotubes during tapping mode imaging on fragile samples, such as a polycrystalline silicon surface. Their tests led to the conclusion that, using a CNT tip, neither the sample nor the probe is affected by the imaging of over 1100 scans. In a later work, Guo *et al* (2005) conducted experiments on wear characteristics of CNT and silicon probes. Their tests led to the conclusions that CNT probes are wear resistant, accordingly featuring a good anti-wear characteristic and a long lifetime, compared to silicon probes; and that CNT tips produce much less damage to the scanned sample when compared to silicon probes.

The mechanical properties of the CNTs have been studied using theoretical and experimental methods. Nonlinear elastic responses and mechanical robustness of nanotubes and nanorods have been analyzed by various researchers (Iijima *et al* 1995, Yacobson *et al* 1997, Falvo *et al* 1997, Wong *et al* 1997, Ru 2000, Belytschko *et al* 2002, Nakajima *et al* 2003). Yu *et al* (2000) analyzed the breaking mechanism of MWNTs under tensile loads, while Daraio *et al* (2004a, 2004b) focused on the dynamic nanofragmentation mechanism, the nonlinear contact interaction and the impact response of carbon nanotube forests. Cao *et al* (2005) reported the fully reversible compressive behavior of CNT films.

Besides the analysis of the mechanical properties, the understanding of the nanotribological behavior, such as the adhesion and the friction, between the CNTs and different materials plays a key role in the exploration of new applications for the CNTs (Bhushan 2002, 2005). Kinoshita *et al* (2004), Turq *et al* (2005) studied the frictional behavior of a vertically aligned carbon nanotubes forest against an atomic force microscope gold tip in air. Their experiments were conducted using a gold tip, under controlled relative humidity varying from 0 to 100%. Due to the nanometer scale of the tip radii and of the applied forces, these studies concern the microtribological characterization of the samples more than their nanometer-scale analysis. Due to the emerging potential application of nanotubes in structures which mimic gecko feet and the lotus effect and in composites in order to achieve different properties, such as the electrical conductivity or the improvement of the mechanical strength of polymer composites, the analysis of the interaction between the CNTs and different materials on a nanometer scale is still needed.

The objective of this paper is to systematically explore the nanotribological properties of carbon nanotubes, both as part of an AFM tip, and organized in vertically aligned arrays. In particular, the objective is to evaluate adhesion and friction properties on the nanoscale using MWNT, Si and Si_3N_4 tips on Si, Al and mica samples, and using Si tips on SWNT and MWNT arrays, and to analyze the wear after tests at two normal loads using the MWNT tip and a Si tip on a gold film, and a Si tip on the SWNT and MWNT arrays.

2. Experimental details

2.1. AFM tips

The multiwalled AFM tip used in this study is shown in figure 1. Low-density and individually separated multiwalled carbon nanotubes (MWNTs) were grown by chemical vapor deposition on a Pt wire coated with a liquid catalyst solution as previously reported (Nguyen *et al* 2005). Using an inverted microscope at 500× magnification, a single MWNT with typical length greater than 10 μm was transferred to the tip of a Si cantilever that was coated with a 15 nm Ni film. The relative

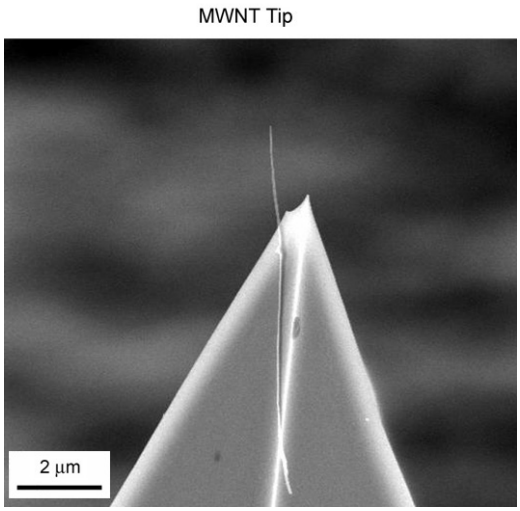

Figure 1. SEM image of the MWNT tip.

position of the MWNT to the Si tip was manually manipulated using a pair of microtranslators. When the nanotube and the Si tip were in close proximity, an electrical potential of 1–2 V was applied in order to improve the alignment of the nanotube with respect to the apex of the Si tip. Once the desired alignment of the nanotube was achieved, the MWNT was detached from its source by increasing the voltage to 10 V and above. The detachment occurs at the point of defects along the length of the MWNT due to Joule heating at this highest electrical resistivity. The applied voltage also caused local heating at the MWNT–Ni-coated Si tip interface, which strengthens the interface perhaps through physical welding of the MWNT to the Ni film and/or the formation of chemical bonds between the MWNT and the Ni-coated Si tip. The diameters of the MWNT tips typically ranged from 10 to 30 nm with a length beyond the silicon structure varying widely from a few μm to tens of μm. The MWNT are open, since their diameter is relatively large for cap closing to occur. The cantilever has a resonance frequency of about 75 kHz and nominal force constant of 2 N m^{-1}. The actual length of the cantilever was measured with an optical microscope to be about 200 μm. The total height of the tip, including the supporting silicon tip structure and the length of the attached MWNT tip, is approximately 17 μm, with the length of the nanotube protruding beyond the Si apex being about 2 μm, as seen in figure 1.

For comparison, a force modulation etched silicon tip (RFESP, Veeco) and silicon nitride tip (NP-S, Veeco) were used for the same measurements of the adhesion force and the coefficient of friction. The RFESP silicon tips are made from a 0.5–2 Ω cm phosphorus (n) doped Si (100) wafer by being cleaned in hot HCl:H_2O_2:DI water, etched in 6:1 HF:DI water buffered with ammonium fluoride, followed by potassium hydroxide, hot phosphoric acid, and then HF etching. After etching, the tips are rinsed in DI water and blow-dried with nitrogen that had flowed through a plastic tube. The length of the cantilever on the tip is 225 μm, its nominal resonance frequency is 75 kHz, and its nominal spring constant is 3 N m^{-1}. The nominal tip height is 15 μm, with a nominal radius of about 10 nm. Silicon nitride tips are held by a cantilever with 115 μm nominal length and 0.58 N m^{-1} nominal spring constant. Their height is in the 2.5–3.5 μm range, and their nominal tip radius is 20–50 nm.

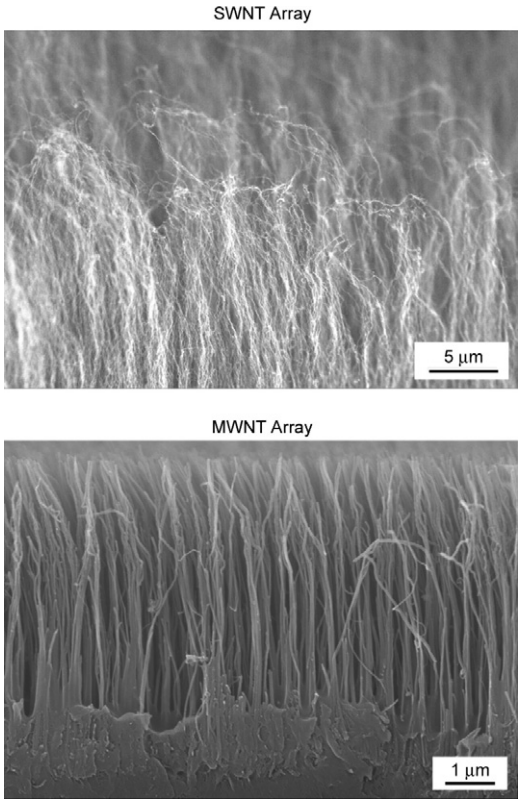

Figure 2. SEM images of the vertically aligned SWNT and MWNT arrays. In the top image bundles of SWNTs are observed.

The tests on the vertically aligned CNTs arrays (to be described later) were performed with two etched silicon tips (RFESP, Veeco).

2.2. Test samples

In order to study the effect of the MWNT tip interacting with different materials, the tests were performed on single-crystal silicon (100), single-crystal aluminum, mica and gold film samples. The first represents a ceramic material, while the second two represent ductile metals. The gold film is 100 nm thick and was deposited on a silicon substrate by evaporation.

For the second part of the study, two different vertically aligned carbon nanotubes arrays were tested (figure 2). One array is composed of SWNTs, with diameter less than 5 nm. The second array is formed by MWNTs, with diameter between 20 and 50 nm. For the two arrays, the lengths of the nanotubes are between 5 and 10 μm. The nanotubes are open with no capping. The aligned SWNTs were synthesized by deposition of ∼1 nm Fe on Al (∼10 nm) coated SiO_2/Si substrate, followed by plasma-enhanced vapor phase deposition (PECVD) (80 W, 13.56 MHz) of ∼30 mTorr C_2H_2 for 10–15 min at 750 °C. After the synthesis, the SWNTs were transferred onto gold film by sputter coating, followed by ∼10% HF aqueous solution etching (Huang *et al* 1999).

The aligned MWNT/polymer sample was prepared according to the method of Qu and Dai (2007). An appropriate polymer thin film, polystyrene (PS) in our case (M_w = 350 000; T_g (glass transition temperature) ≈ 105 °C; T_m (melting point) ≈ 180 °C; T_c (decomposition temperature) ≈ 350 °C; thickness: ∼50 μm) was first placed on the top surface of a vertically aligned carbon nanotube array (Huang *et al* 1999). By heating the SiO_2/Si substrate by an underlying hot plate to a temperature above T_m and below T_c, the melted PS film gradually infiltrated the nanotube forest through a combined effect of gravity and capillary forces. The infiltration depth (i.e., the embedment length) of PS into the nanotube forest depends strongly on the temperature and heating time. After a predetermined heating time, the polymer-infiltrated nanotube array was peeled off from the SiO_2/Si substrate in an aqueous solution of HF (10% wt) to generate a free-standing film of vertically aligned carbon nanotubes embedded into the PS matrix.

2.3. Adhesive force, friction force, and wear measurements

Adhesive and friction forces were measured using a MultiMode AFM (Digital Instruments, Santa Barbara, CA). The friction measurements with the Si and Si_3N_4 tips were carried out on a 2 μm scan line, with a 4 μm s^{-1} tip velocity (corresponding to 1 Hz scan rate) and 90° scan angle, with applied normal load ranging from 0 to 250 nN. Three sets of measurements for each tip on each sample were performed, increasing and decreasing the applied load three times (Bhushan 2005). The corresponding coefficients of friction were evaluated following method 2 presented by Ruan and Bhushan (1994). The coefficient of friction is obtained from the slope of the average TMR (trace minus retrace) versus normal load curves, whose values are monitored during the scan of the tip perpendicularly to the cantilever long axis direction. With the carbon nanotube tip, the same settings were used, except for the scan angle, which was kept at 0° in order to scan the tip parallel to the cantilever long axis direction as required by method 1 in Ruan and Bhushan (1994). The coefficients of friction were obtained from the slope of the average TMR versus Z central position value. Friction data were collected for three loading and unloading cycles at three different locations for each sample.

The wear tests were performed on a 2 μm × 2 μm area, with a scan velocity of 4 μm s^{-1}, corresponding to a scan rate of 1 Hz, with a normal load applied to the cantilever of 100 and 200 nN (Bhushan 2005). In order to analyze the sample wear, the surfaces were scanned in the tapping mode after each test. To measure the tip wear, the method proposed by Tao and Bhushan (2006a) was followed. When scanning an isolated structure that is much sharper than the tip, the resulting image is a scan of the tip itself. Therefore, a silicon TGT1 grating sample (NTMDT, Moscow, Russia) was scanned with the CNT tip and one of the etched silicon tips for the preliminary tip characterization. The grating sample has an array of sharp tips on the surface, arranged on each corner and the center of a 3 × 3 μm^2 square. The height of each tip is 0.4 μm, the tip angle is about 30°, and the radius is less than 10 nm. The scanning was performed on a 2 μm × 2 μm area, at an average tip velocity of 2 μm s^{-1}, corresponding to a 0.5 Hz scan rate, in the direction parallel to the cantilever axis. SPIP software (Image Metrology A/S, Denmark) was used to characterize the tips used for the tests, and to evaluate their radii and cone angles. The image was obtained by scanning the TGT1 grating sample, then the surfaces of the tips were generated using a blind tip reconstruction algorithm from the scanning image. A 2D profile was generated from the tip surface for each tip. The characterization of the shape of the MWNT tip using the SPIP software could not be carried out due to the structure of the nanotube. Since its end is open, its radius is infinite. Therefore it is not possible to image it using the silicon grating.

All experiments were performed in ambient conditions, at 22 ± 1 °C and 45–55% relative humidity.

3. Results and discussion

3.1. Adhesive forces and friction measurements

3.1.1. MWNT tip on Si, Al and mica samples. The force calibration plots obtained from our measurements of adhesive forces, reported in figure 3(a), show a nonlinear behavior that can be related to the effects of the tip–surface interactions. The nanotube on the tip comes in contact with the surface (point A). As the tip continues to be pressed, the contact forces cause the linear deflection of the cantilever. After this initial bending, as the tip travels toward the sample (from B to C), the cantilever deflection (load) remains almost constant, with some variation. A similar nonlinear behavior has been observed when operating the AFM in tapping mode by Lee *et al* (2004). The nonlinear behavior indicates that, as the tip is continuously pushed into the surface, it induces the MWNT to bend and buckle, and the nanotube deflection is more than the cantilever deflection (figure 3(b)). It is noted that, during buckling, the graphitic C–C bonds, more specifically the π and σ bonds along the sp^2 hybridized chains, transform from the sp^2 to the sp^3 hybrid form when a mechanical stress is imposed along the nanotube axis. Such transformation is due to the breakage of the π C–C bonds, and it is reversible since the sp^2 C–C bonds are more thermodynamically stable than the sp^3 bonds (Tombler *et al* 2000). The nanotube buckles until the applied force reaches the Euler buckling force (Young and Roark 2001):

$$F_{\text{Euler}} = (\pi^2 EI)/L^2 \tag{1}$$

where E is the MWNT Young's modulus (∼1 TPa, (Wong *et al* 1997)), I is the area moment of inertia ($I = \pi(r_2^4 - r_1^4)/4$, where r_1 and r_2 are the inner and outer radii of the nanotube, $r_2 \sim 10$ nm for the tip) and L is the nanotube length (∼2 μm). Above the buckling force, the MWNT becomes unstable and buckles sideways, and it lies on the surface and slides. The buckling force for the nanotube tip under study was calculated to be about 20 nN. This suggests that, since the load being applied at point B (∼100 nN) is on the order of the buckling force, the nanotube buckles from point B to C and lies sideways. Friction between the nanotube and the surface with some roughness and continuous bending of the nanotube is responsible for the variations observed from point B to C.

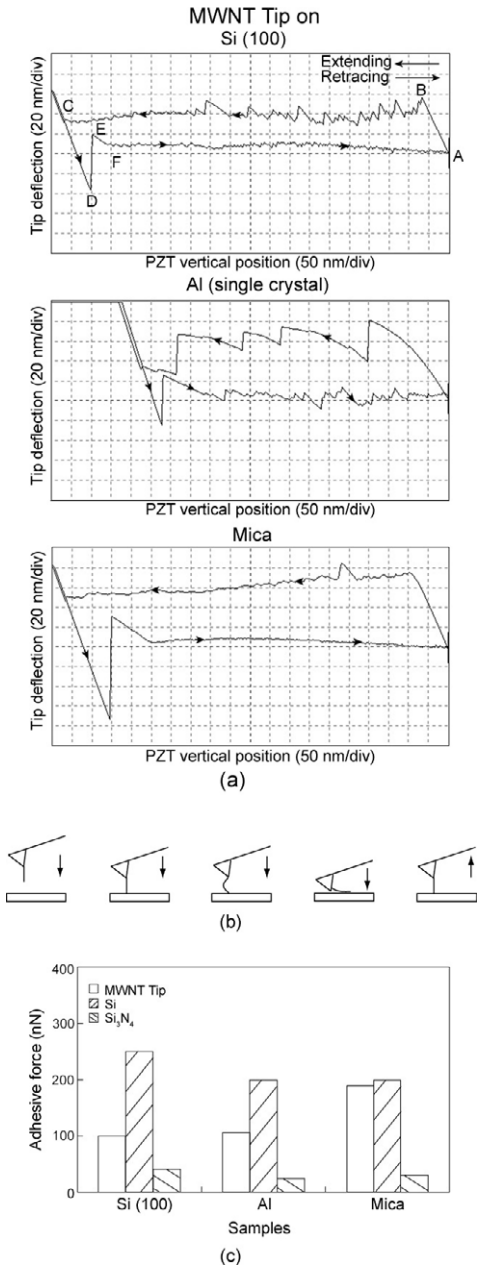

Figure 3. (a) Force calibration plots using the MWNT tip on the Si, Al, and mica samples, (b) schematic of the buckling of the MWNT tip during the force calibration, and (c) mean values of the adhesive forces for various tips on three samples. The σ values are about 20% of the mean values.

At point C, the silicon tip supporting the MWNT snaps into contact with the surface, inducing a linear deflection of the cantilever. When the tip is retracted by the piezo (point D), the elastic force of the cantilever overcomes the adhesion between the tip and the sample, and the tip jumps out of contact (point E). Once the silicon tip jumps out of contact (point E), the elastic energy stored by the MWNT is released (from E to F). After that, the bent MWNT will gradually unload its stress accumulated earlier in the extending regime, when the tip continuously moves away from the sample. This process is expected to generate a repulsive force comparable to that in the extending regime as shown by Lee *et al* (2004). However, this is in contradiction to what we observed, since the cantilever deflection during the retracting regime F–A is significantly lower than that during the extending regime B–C. The discrepancy here is explained by the change in sliding direction between the MWNT and the sample. The friction force reverses its direction when the silicon tip is detached from the sample surface, reducing the stress stored in the MWNT instead of increasing it during the extending regime B–C. In addition, the deflection at point E is just in the middle of point C and point F, corresponding to an intermediate status before the friction force reverses its direction.

Table 1. Summary of adhesive forces and coefficient of friction for various tips on Si, Al and mica samples.

	F_{adh} (nN)			Coefficient of friction		
	Tips			Tips		
Sample	MWNT	Si	Si_3N_4	MWNT	Si	Si_3N_4
Si	100	250	40	0.05	0.05	0.05
Al	107	200	25	0.04	0.05	0.04
Mica	190	200	30	0.06	0.05	0.04

From the force calibration plots, the adhesion forces have been estimated (obtained by multiplying the horizontal distance between the crossing points of the force plot with the zero line to the cantilever stiffness), and the corresponding values are reported in table 1. It is a joint contribution from the adhesion between the silicon tip supporting the MWNT tip and the bent MWNT tip with the sample as well as the elastic stresses stored in the bent MWNT. Although we cannot exclude the possibility that, during the jumping-out event, the MWNT lying on the sample surface might be slightly peeled off, the contribution to the measured adhesion from peeling of the MWNT can be safely neglected since the peeling length should be no longer than the jumping-out distance of 50 nm, which is much smaller than the length of the MWNT itself $\sim$2 μm. Moreover, as reported by Barber *et al* (2004), CNTs have a contact angle of about 80°, and they are better wetted by water than graphite because of their higher polar energy component, but their structure is still hydrophobic. Therefore, any interactive capillary forces from the peeled segment of the MWNT tip should not make a large contribution to the observed adhesive forces.

For comparison, the adhesive forces have also been estimated using a Si and a Si_3N_4 tip, and the data are presented in figure 3(c). The adhesion experienced by the silicon tip is the highest. This can be explained with the higher capillary force to which silicon is subjected due to its low contact angle of 51° (Tao and Bhushan 2006a). Silicon nitride is characterized by a contact angle of 48° (Tao and Bhushan 2006b); therefore the adhesive force should have a magnitude compared to the one observed for the silicon tip. The difference in the adhesion may be related to the differences in surface energy based on the well-known surface energy theory of adhesion (Bhushan 2002, 2003).

For the MWNT tip sliding on different samples, the coefficients of friction have been evaluated, and the data are

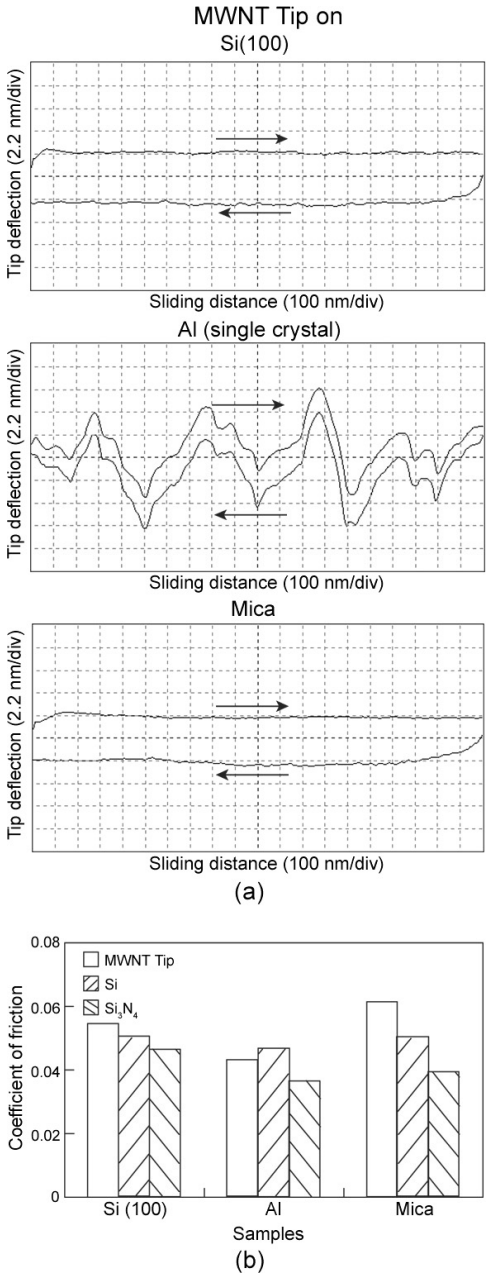

Figure 4. (a) Vertical deflection of the MWNT tip on the Si, Al, and mica samples, sliding along the longitudinal axis of the cantilever beam for the friction measurements at a constant load (100 nN), (b) mean values of coefficients of friction for various tips on three samples. The σ values are about 15% of the mean values.

presented in figure 4 and table 1. The coefficients of friction evaluated with the MWNT tip on the silicon and the mica surfaces are slightly higher than the values measured using the Si and the Si_3N_4 tips. Such a trend can be due to the surface chemistry and the bending of the nanotube during the scan. As the tip is pushed against the surface, the nanotube buckles and bends laterally, leading to an increase of the contact area, which causes higher resistance to tip motion. In the case of the Al sample, the large variation of lateral deflection signals appears to be the consequence of the high surface roughness (Bhushan 2002).

Table 2. Summary of adhesive forces and coefficient of friction for two Si tips on SWNT and MWNT arrays.

	F_{adh} (nN)		Coefficient of friction	
	Tips		Tips	
Sample	Si_1	Si_2	Si_1	Si_2
SWNT	86	96	0.29	0.20
MWNT	94	96	0.32	0.24

3.1.2. Si tip on SWNT and MWNT arrays. The adhesion experiments were performed on the SWNT and the MWNT arrays, whose AFM images are shown in figure 5. The data are presented in figure 6 and table 2. Based on the adhesion force values presented in figure 6(b) and table 2, the values are slightly lower for the SWNT array as compared to those for the MWNT array.

The force calibration curves of the Si tip on the SWNT and MWNT arrays are shown in figure 6(a). From those force plots it can be observed that, once the engagement occurs with the surface and the tip is pushed further, the cantilever is smoothly deflected until the piezo retraces in a nonlinear pattern, in contrast to the linear pattern we usually observe on homogeneous samples. This can be explained as follows. As the tip is pushed further down in the array, more nanotubes get into contact with the tip, gradually contributing to repulsion. This condition is reversed when the tip is retracted from the arrays, leading to a nonlinear detaching curve. The source of the adhesive force is van der Waals forces in the contact of the tip with many carbon nanotubes or with a large contact area between the tip and a single nanotube due to its flexibility. Although the nanotubes are hydrophobic, the capillary force may still play a role in the adhesion between the silicon tip and the nanotube arrays due to the high surface energy of the nanotubes (Lau *et al* 2003). It has been shown that nanotube forests, with a 10–15 μm length, have an initial water contact angle of 161°; however, the droplets are not stable and eventually seep into the forest voids after a few minutes. For shorter CNTs, water droplets immediately seep into the voids, and the nanotubes are even forced into bundles under the surface tension effects of the evaporating water between the nanotubes, reducing their hydrophobicity. The force calibration plots monitored in our studies are similar to the ones presented by Decossas *et al* (2001) in their tests on an MWNT carpet (where the nanotubes are not aligned) with a silicon nitride tip, and the plots reported by Yurdumakan *et al* (2005), obtained by scanning a silicon tip on an MWNT array. A lot of variability in the value of the adhesion has been observed, and it is expected to be due to the different nanotube arrangements in different points of the samples including the packing density (figure 5).

The friction data measured on the SWNT and the MWNT arrays are reported in table 2 and shown in figure 7. The SWNT array showed a lower coefficient of friction than the MWNT array, similar to the trends observed for the adhesion forces. Besides the density difference, the higher stiffness of the MWNTs, compared to the SWNTs, may contribute to the high friction. SWNTs

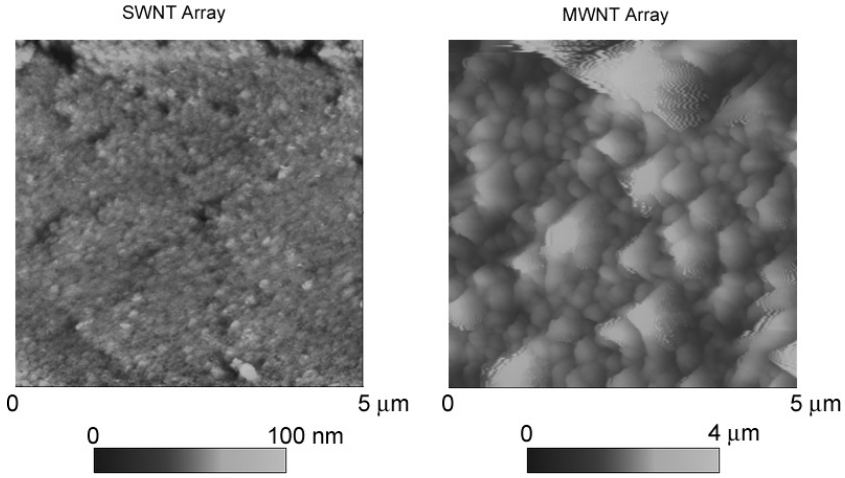

Figure 5. Tapping mode topographical images of the SWNT and the MWNT arrays using a Si tip.

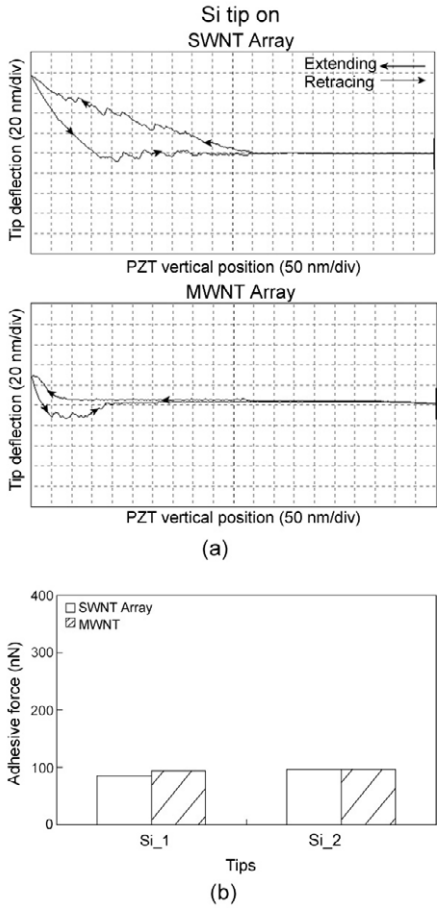

Figure 6. (a) Force calibration plots of the Si tip on the SWNT and the MWNT arrays, (b) mean values of the adhesive forces measured with two different Si tips. The σ values are about 40% of the mean values.

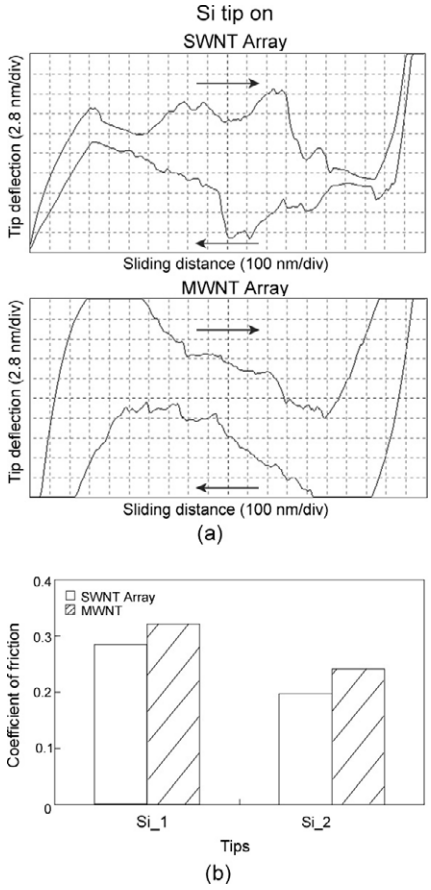

Figure 7. (a) Lateral deflection of the Si tip on the SWNT and the MWNT arrays sliding along the axis orthogonal to the long axis of the cantilever beam for friction measurements, (b) mean values of the coefficients of friction measured with two different Si tips. The σ values are about 20% of the mean values.

have a smaller bending force constant, since their diameter is smaller; thus they are mechanically more flexible than MWNTs and offer less resistance to the motion of the tip.

Some influence may also occur by the cohesion forces between the nanotubes on the array, which is expected to be higher on the MWNT array since the nanotube density is higher than the density of the SWNT vertical array.

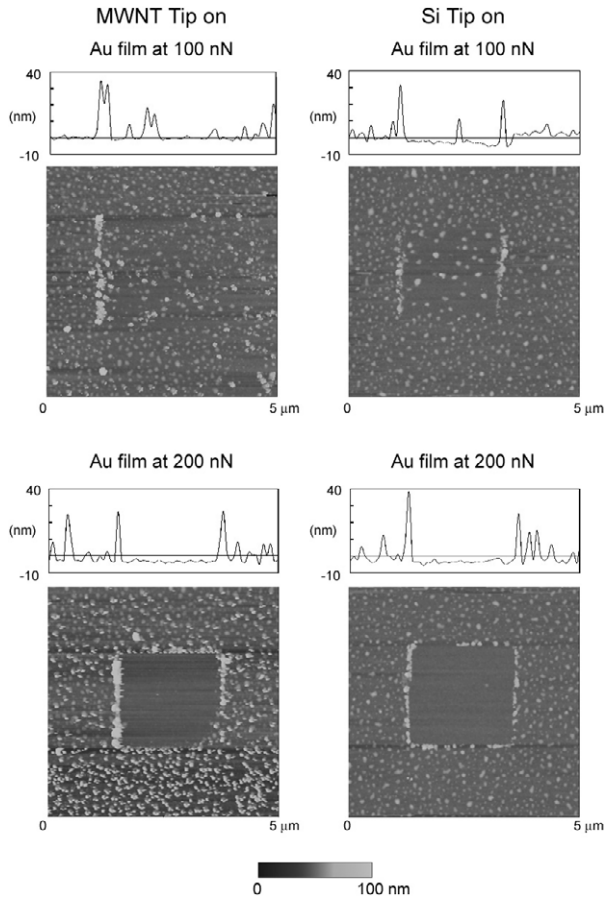

Figure 8. Tapping mode topographical images of the gold film after the wear test with the MWNT tip (in the left column) and the Si tip (in the right column) after 100 nN and 200 nN normal loads for 10 min.

3.2. Wear tests

3.2.1. MWNT and Si tip on Au film sample. The wear maps on the gold film are shown in figure 8. It is noted that the wear induced on the surface after the 100 nN normal load tests is very low; the material was pushed in the sliding direction of the tip. The topographical changes are more evident on the sample worn with the Si tip. In particular, it is hard to quantify a wear depth on the sample scanned with the MWNT tip, while the wear depth induced by the silicon tip is quantifiable and is about 3 nm. Low wear using the MWNT tip can possibly be due to the buckling of the carbon nanotube during the scan, which may be absorbing some of the force at contact, acting as a compliant spring moderating the impact of the tip on the surface (Larsen *et al* 2002, Nguyen *et al* 2005). Moreover, the smaller tip radius of the MWNT tip compared to the Si tip results in less contact area to the surface, which consequently does less damage (Bhushan 2002, Guo *et al* 2005). By applying a 200 nN load, the damages induced to the gold film are about the same for the two tips used and the average wear depths are about 5 nm for both the MWNT and the Si tips. This result may suggest that under such normal load the silicon tip holding the MWNT may also be in contact with the surface, resulting in the similar wear behavior.

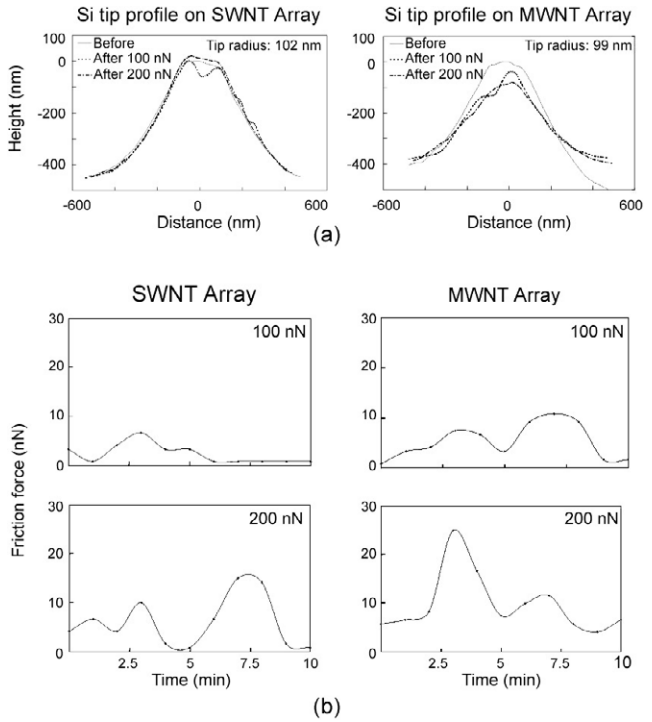

Figure 9. (a) Surface profiles of the Si tip before and after the wear tests on the SWNT and the MWNT arrays, and (b) mean values of friction force profiles obtained during the wear tests on the SWNT and the MWNT arrays. During the tests, the tip was slid orthogonal to the long axis of the cantilever beam.

3.2.2. Si tip on SWNT and MWNT arrays. The surface topographical images of the SWNT and the MWNT arrays captured after the wear tests are the same as in figure 5, indicating that no damage was caused on either sample. The tip profiles before and after the wear tests are presented in figure 9(a). From this figure, it is possible to see how the Si tip wears. Whereas the changes in the shape of the tip are negligible on the SWNT array after the 100 and 200 nN tests, the shape of the tip changes with the MWNT array. It appears that the Si tip profile after tests with the MWNT array at 100 nN load gets sharper, which may be due to material pick-up. The flattening of the profiles at a distance of about 300 nm may occur due to artifacts in the silicon grating sample. Next, the wear volume of the tip generated by the MWNTs was calculated according to the procedure developed by Tao and Bhushan (2006a), and was found to be 34×10^4 nm^3 after the 100 nN normal load tests, and 51×10^4 nm^3 after the 200 nN normal load experiments. These values are comparable to the values reported by Tao and Bhushan (2006a) for Si tips on Si at 100–200 nN normal load.

The friction force values obtained during the wear tests are reported in figure 9(b). The mean value of the friction force during the entire experiment is higher when the tip is scanned on the MWNT array. It is therefore reasonable to expect wear on the tip after the tests conducted on that sample. The differences in the interactions with the SWNTs and MWNTs, and the fluctuations, have been discussed earlier in section 3.1.2.

4. Conclusions

In this study, a comprehensive investigation of adhesion, friction and wear of carbon nanotubes has been carried out.

By investigating the adhesion, it is concluded that when the MWNT tip is brought in and out of contact with the surface, nonlinear behavior is observed mainly due to the bending and buckling, resulting in high contact area and the sliding of the nanotube on the surface. Moreover, relatively high values for the adhesive force have been observed, and this is believed to be due to a contribution from the silicon tip, holding the MWNT tip, contacting the surface. The bending and buckling of the nanotube, in addition to the surface chemistry, may also be the reason for the slightly higher coefficient of friction observed with the MWNT tip, with respect to the values recorded for the Si and the Si_3N_4 tips on silicon (100), single-crystal aluminum and mica surfaces. When the nanotube bends, it results in a larger contact area, which causes a higher resistance to the motion.

The adhesive forces evaluated between the Si tips and the SWNT and the MWNT arrays showed a lot of variability. This is believed to be related to the density and the arrangement of the nanotubes at the interface. Moreover, the relatively high values of such forces observed on the MWNT array can be due to the presence of large van der Waals forces related to the contact of the tip with numerous nanotubes, or to a large contact area between the tip and a single nanotube. The coefficient of friction estimated for the SWNT array is lower than the one corresponding to the MWNT array. Such observation can be the consequence of lower van der Waals forces and the larger flexibility of the single-walled nanotubes, which is less resistive to the motion.

The wear tests conducted on the gold film at two normal loads show the low damage induced by the lower load when the MWNT tip is used. This may be related to the buckling of the nanotube, which acts as a compliant spring, adsorbing part of the force transmitted by the cantilever. When the 200 nN load is applied, no difference in the wear traces can be observed on the surface scanned with either tip. It can then be concluded that such a load may bring the silicon tip, holding the MWNT tip, into contact with the substrate.

Wear tests were carried out on the SWNT and the MWNT arrays using the Si tip, and their topographical images did not show any change. The tip showed a negligible wear after the test on the SWNT array. On the contrary, a larger tip wear in the MWNT array can be observed. This is consistent with the friction forces monitored during the test: the mean value of the friction force between the tip and the SWNTs is slightly lower than the one recorded for the MWNTs. It can be concluded that the larger flexibility of the SWNTs plays a key role in the interaction with the tip, allowing the nanotubes to bend more rather than to oppose the tip motion, and consequently reducing tip wear.

Acknowledgments

Barbara Galasso acknowledges a fellowship provided by the Politecnico di Torino in order to carry out research at The Ohio State University. She would also like to thank the NLIM researchers for helpful discussions, in particular Drs Xing Ling and Manuel L Palacio.

References

An J-W, You D-H and Lim D-S 2003 Tribological properties of hot-pressed alumina-CNT composites *Wear* **255** 677–81

Barber A H, Cohen S R and Wagner H D 2004 Static and dynamic wetting measurements of single carbon nanotubes *Phys. Rev. Lett.* **92** 186103–4

Baughman R H, Zakhidov A A and de Heer W A 2002 Carbon nanotubes—the route toward applications *Science* **297** 787–92

Belytschko T, Xiao S P, Schatz G C and Ruoff R S 2002 Atomistic simulation of nanotube fracture *Phys. Rev.* B **65** 235430

Bhushan B 2002 *Introduction to Tribology* (New York: Wiley)

Bhushan B 2003 Adhesion and stiction: mechanisms, measurement techniques, and methods for reduction *J. Vac. Sci. Technol.* B **21** 2262–96

Bhushan B 2005 *Nanotribology and Nanomechanics, An Introduction* (Berlin: Springer)

Bhushan B 2007 *Handbook of Nanotechnology* 2nd edn (Berlin: Springer)

Bhushan B, Kasai T, Nguyen C V and Meyyappan M 2004 Multiwalled carbon nanotube AFM probes for surface characterization of micro/nanostructures *Microsyst. Technol.* **10** 633–9

Biercuk M J, Llaguno M C, Radosavljevic M, Hyun J K, Johnson A T and Fisher J E 2002 Carbon nanotube composites for thermal management *Appl. Phys. Lett.* **80** 2767–9

Cao A, Dickrell P L, Sawyer W G, Ghasemi-Nejhad M N and Ajayan P M 2005 Super-compressible foamlike carbon nanotube films *Science* **310** 1307–10

Chen W X, Tu J P, Wang L Y, Gan H Y, Xu Z D and Zhang X B 2003 Tribological application of carbon nanotubes in a metal-based composite coating and composites *Carbon* **41** 215–22

Chen X H, Chen C S, Xiao H N, Liu H B, Zhou L P, Li S L and Zhang G 2006 Dry friction and wear characteristics of nickel/carbon nanotube electroless composite deposits *Tribol. Int.* **39** 22–8

Chen Y, Shaw D T and Guo L 2000 Field emission of different oriented carbon nanotubes *Appl. Phys. Lett.* **76** 2469–71

Dai H, Hafner J H, Rinzler A G, Colbert D T and Smalley R E 1996 Nanotubes as nanoprobes in scanning probe microscopy *Nature* **384** 147–50

Dai L, He P and Li S 2003 Functionalized surfaces based on polymers and carbon nanotubes for some biomedical and optoelectronic applications *Nanotechnology* **14** 1081–97

Daraio C, Neterenko V F, Aubuchon J F and Jin S 2004a Dynamic nanofragmentation of carbon nanotubes *Nano Lett.* **4** 1915–8

Daraio C, Neterenko V F and Jin S 2004b Highly nonlinear contact interaction and dynamic energy dissipation by forest of carbon nanotubes *Appl. Phys. Lett.* **85** 5724–6

de Heer W A, Bacsa W S, Châtelain A, Gerfin T, Humphrey-Baker R, Forro L and Ugarte D 1995 Aligned carbon nanotube films: production and optical and electronic properties *Science* **268** 845–7

Decossas S, Cappello G, Poignant G, Patrone L, Bonnot A M, Comin F and Chevrier J 2001 Interaction forces between carbon nanotubes and an AFM tip *Europhys. Lett.* **53** 742–8

Dong S R, Tu J P and Zhang X B 2001 An investigation of the sliding behavior of Cu-matrix composite reinforced by carbon nanotubes *Mater. Sci. Eng.* A **313** 83–7

Dresselhaus M S *et al* 2000 *Carbon Nanotubes: Synthesis, Structure, Properties, and Applications* (Berlin: Springer)

Ebbesen T W and Ajayan P M 1992 Large-scale synthesis of carbon nanotubes *Nature* **358** 220–2

Falvo M R, Clary G J, Taylor R M II, Chi V, Brooks F P Jr, Washburn S and Superfine R 1997 Bending and buckling of carbon nanotubes under large strain *Nature* **389** 582–4
Fan S, Chapline M G, Franklin N R, Tombler T W, Cassel A M and Dai H 1999 Self-oriented regular arrays of carbon nanotubes and their field emission properties *Science* **283** 512–4
Guo L, Wang R, Xu H and Liang J 2005 Wear-resistance comparison of carbon nanotubes and conventional silicon-probes for atomic force microscopy *Wear* **258** 1836–9
Huang L, Lau S P, Yang H Y, Leong E S P, Yu S F and Prawer S 2005 Stable superhydrophobic surface via carbon nanotube coated with ZnO thin film *J. Phys. Chem.* B **109** 7746–8
Huang S D, Dai L and Mau A W H 1999 Patterned growth and contact transfer of well-aligned carbon nanotube films *J. Phys. Chem.* B **103** 4223–7
Iijima S 1991 Helical microtubules of graphitic carbon *Nature* **354** 56–8
Iijima S and Ichihashi T 1993 Single-shell carbon nanotubes of 1nm diameter *Nature* **363** 603–6
Iijima S, Brabec C, Maiti A and Bernholc J 1995 Structural flexibility of carbon nanotubes *J. Chem. Phys.* **104** 2089–92
Kim P and Lieber C M 1999 Nanotube nanotweezers *Science* **286** 2148–50
Kinoshita H, Kume I, Tagawa M and Ohmae N 2004 High friction of a vertically aligned carbon-nanotube film in microtribology *Appl. Phys. Lett.* **85** 2780–1
Kong J, Franklin N R, Zhou C, Chapline M G, Peng S, Cho K and Dai H 2000 Nanotube molecular wires as chemical sensors *Science* **287** 622–5
Larsen T, Moloni A, Flack F, Eriksson M A, Lagally M G and Black C T 2002 Comparison of wear characteristics of etched-silicon and carbon nanotube atomic-force microscopy probes *Appl. Phys. Lett.* **80** 1996–8
Lau K K S, Bico J, Teo K B K, Chhowalla M, Amaratunga G A J, Milne W I, McKinley G H and Gleason K K 2003 Superhydrophobic carbon nanotube forest *Nano Lett.* **3** 1701–5
Lee H, Mall S, He P, Shi D, Narasimhadevara S, Yeo-Heung Y, Shanov V and Shulz M J 2007 Characterization of carbon nanotube/nanofiber-reinforced polymer composites using an instrumented indentation technique *Composites* B **38** 58–65
Lee S I, Howell S W, Raman A, Reifenberger R, Nguyen C V and Meyyappan M 2004 Nonlinear tapping dynamics of multi-walled carbon nanotube tipped atomic force microcantilevers *Nanotechnology* **15** 416–21
Li X, Guan W, Yan H and Huang L 2004 Fabrication and atomic force microscopy/friction force microscopy (AFM/FFM) studies of polyacrylamide-carbon nanotubes (PAM-CNTs) copolymer thin films *Mater. Chem. Phys.* **88** 53–8
Nakayama Y and Akita S 2001 Field-emission device with carbon nanotubes for a flat panel display *Synth. Met.* **117** 207–10
Nakajima M, Arai F, Dong L and Fukua T 2003 Measurements of the bi-linear elasticity of identical carbon nanotubes *Nanotechnology* **1** 156–9
Nguyen C V, Chao K-J, Stevens R M D, Delzeit L, Casel A, Han J and Meyyappan Y 2001 Carbon nanotube tip probes: stability and lateral resolution in scanning probe microscopy and application to surface science in semiconductors *Nanotechnology* **12** 363–7
Nguyen C V, So C, Stevens R M, Li Y, Delziet L, Sazzani P and Meyyappan M 2004 High lateral resolution scanning probe with sharpened tip of multi-walled carbon nanotube scanning probe *J. Phys. Chem.* B **108** 2816–21
Nguyen C V, Ye Q and Meyyappan M 2005 Carbon nanotube tips for scanning probe microscopy: fabrication and high aspect ration nanometrology *Meas. Sci. Technol.* **16** 2138–46
Nygård J, Cobden D H and Lindelof P E 2000 Kondo physics in carbon nanotubes *Nature* **408** 342–6
Pambaguian L, Edtmainer C, Janhsen T, Ferrato M, Chereau P, Forero S, Frey T, Girmscheid A, Heibig J, Hepp F, Peigney A, Laurent C and Wulz H G 2007 Non-organic matrix materials reinforced with carbon nanotubes for space applications *Proc. Viennano'07* ed W Bartz *et al*, pp 31–40
Peigney A, Flahaut E, Laurent C, Chastel F and Rousset A 2002 Aligned carbon nanotubes in ceramic-matrix nanocomposites prepared by high-temperature extrusion *Chem. Phys. Lett.* **352** 20–5
Qu L and Dai L 2007 Polymer-masking for controlled functionalization of carbon nanotubes *Chem. Commun.* **2007** 3859–61
Quian D, Dickey E C, Andrews R and Ranell T 2000 Load transfer and deformation mechanism in carbon nanotube–polystyrene composites *Appl. Phys Lett.* **76** 2868–70
Ru C Q 2000 Effective bending stiffness of carbon nanotubes *Phys. Rev.* B **62** 9973–6
Ruan J and Bhushan B 1994 Atomic-scale friction measurements using friction force microscopy: part I-general principles and new measurement techniques *ASME J. Tribol.* **116** 378–88
Schadler L S, Giannaris S C and Ajayan P M 1998 Load transfer in carbon nanotube epoxy composites *Appl. Phys. Lett.* **73** 3842–4
Shaikh S, Lafdi K and Silverman E 2007 The effect of a CNT interface on the thermal resistance of contacting surfaces *Carbon* **45** 696–703
Shi D, Lian J, He P, Wang L M, Xiao F, Yang L, Schulz M J and Mast D B 2003 Plasma coating of carbon nanofibers for enhanced dispersion and interfacial bonding in polymer composites *Appl. Phys. Lett.* **83** 5301–3
Siegel R W, Chang S K, Ash B J, Stone J, Ajan P M, Doremus R W and Schadler L S 2001 Mechanical behaviour of polymer and ceramic matrix nanocomposites *Scr. Mater.* **44** 2061–614
Snow E S, Campbell P M and Novak J P 2002 Single-wall carbon nanotube atomic force microscope probes *Appl. Phys. Lett.* **80** 2002–4
Tao Z and Bhushan B 2006a Wetting properties of AFM probes by means of contact angle measurements *J. Phys. D: Appl. Phys.* **39** 3858–62
Tao Z and Bhushan B 2006b Surface modification of AFM Si_3N_4 probes for adhesion/friction reduction and imaging improvement *ASME J. Tribol.* **128** 865–75
Tombler T W, Zhou C, Alexseyev L, Kong J, Dai H, Liu L, Jayanthi C S, Tang M and Wu S-Y 2000 Reversible electromechanical characteristics of carbon nanotubes under local-probe manipulation *Nature* **405** 769–72
Turq V, Ohmae N, Martin J M, Fontaine J, Kinoshita H and Loubet J L 2005 Influence of humidity on microtribology of vertically aligned carbon nanotube film *Tribol. Lett.* **19** 23–8
Wang L Y, Tu J P, Chen W X, Wang Y C, Lu X K, Olk C, Cheng D H and Zhang X B 2003 Friction and wear behavior of electroless Ni-based CNT composite coatings *Wear* **254** 1289–93
Wong E W, Sheenan P E and Lieber C M 1997 Nanobeam mechanics: elasticity, strength and toughness of nanorods and nanotubes *Science* **277** 1971–5
Yacobson B I, Campbell M P, Brabec C J and Bernholc J 1997 High strain rate fracture and C-chain unraveling in carbon nanotubes *Comput. Mater. Sci.* **8** 341–8
Yang Z, Dong B, Huang Y, Liu L, Yan F-Y and Li H-L 2005 A study on carbon nanotubes reinforces poly(methyl methacrylate) nanocomposites *Mater. Lett.* **59** 2128–32
Young W C and Roark R J 2001 *Roark's Formulas for Stress and Strain* 6th edn (New York: McGraw-Hill)
Yu M-F, Lourie O, Dyer M J, Moloni K, Kelly T F and Ruoff R S 2000 Strength and breaking mechanism of multiwalled carbon nanotubes under tensile load *Science* **287** 637–40
Yurdumakan B, Raravikar N R, Ajayan P M and Dhinojwala A 2005 Synthetic gecko foot-hairs from multiwalled carbon nanotubes *Chem. Commun.* **2005** 3799–801
Zhou S-M, Zhang X-B, Ding Z-P, Min C-Y, Xu G-L and Zhu W-M 2007 Fabrication and tribological properties of carbon nanotubes reinforced Al composites prepared by pressureless infiltration technique *Composites* A **38** 301–6
Zhu L, Xiu Y, Xu J, Tamirisa P A, Hess D W and Wong C-P 2005 Superhydrophobicity on two-tier rough surfaces fabricated by controlled growth of aligned carbon nanotube arrays coated with fluorocarbon *Langmuir* **21** 11208–12